Monatshefte für Chemie 130, 1047–1059 (1999)

Monatshefte für Chemie
Chemical Monthly

Printed in Austria

Correlation of O–H Stretching Frequencies and O–H···O Hydrogen Bond Lengths in Minerals

Eugen Libowitzky

Institut für Mineralogie und Kristallographie, Universität Wien – Geozentrum, A-1090 Vienna, Austria

Summary. A correlation of O–H stretching frequencies (from infrared spectroscopy) with O···O and H···O bond lengths (from structural data) of minerals was established. References on 65 minerals yielded 125 data pairs for the d(O···O)-v correlation; due to rare or inaccurate data on proton positions, only 47 data pairs were used for the d(H···O)-v correlation. The data cover a wide range of wavenumbers from 1000 to 3738 cm^{-1} and O···O distances from 2.44 to 3.5 Å. They originate from silicates, (oxy)hydroxides, carbonates, sulfates, phosphates, and arsenates with OH^-, H_2O, or even $H_3O_2^-$ units forming very strong to very weak H bonds. The correlation function was established in the form $v(cm^{-1}) = 3592–304 \cdot 10^9 \cdot \exp(-d(O\cdots O)/0.1321)$, $R^2 = 0.96$. Because of deviations from ideal straight H bonds, *i.e.* bent or bifurcated geometry, dynamic proton behavior, but also due to factor group splitting and cationic effects, data scatter considerably around the regression line. The trends of previous correlation curves and of theoretical considerations were confirmed.

Keywords. Correlation diagram; Hydrogen bond length; Infrared spectroscopy; Mineral structure; Stretching frequency.

Korrelation von O–H-Streckfrequenzen und O–H···O-Wasserstoffbrückenlängen in Mineralen

Zusammenfassung. Eine Korrelation zwischen O–H-Streckfrequenzen (aus IR-spektroskopischen Messungen) und O···O- sowie H···O-Bindungslängen (aus Strukturdaten) von Mineralen wurde erstellt. Literaturzitate über 65 Minerale lieferten 125 Datenpaare für die d(O···O)-v-Korrelation. Aufgrund seltener oder ungenauer Daten über Wasserstoffpositionen konnten nur 47 Datenpaare für die d(H···O)-v-Korrelation verwendet werden. Die Daten decken einen weiten Wellenzahlbereich von 1000 bis 3738 cm^{-1} und O···O-Bindungslängen von 2.44 bis 3.5 Å ab. Sie entstammen Silikaten, (Oxi)hydroxiden, Karbonaten, Sulfaten, Phosphaten und Arsenaten mit OH^-, H_2O, oder sogar $H_3O_2^-$ Gruppen, welche sehr starke bis sehr schwache Wasserstoffbrücken ausbilden. Die Korrelationsfunktion wurde in der Form $v(cm^{-1}) = 3592–304 \cdot 10^9 \cdot \exp(-d(O\cdots O)/0.1321)$, $R^2 = 0.96$ erstellt. Aufgrund von Abweichungen von idealen gestreckten H-Brücken, d.h. geknickter oder gegabelter Geometrie, dynamischem Verhalten der Protonen, aber auch wegen Faktorgruppenaufspaltung und Kationeneffekten, streuen die Daten beachtlich um die Regressionslinie. Die Trends früherer Korrelationskurven und theoretischer Berechnungen wurden bestätigt.

Introduction

Hydrogen bonds are usually classified according to bond length, *i.e.* $d(O\cdots O)$, $d(H\cdots O)$, or even d(O–H), and bond strength. The latter is conveniently expressed by the fundamental stretching frequency v of the O–H bond which is easily obtained by infrared (IR) and *Raman* spectroscopy. Thus, very strong H bonds are observed at wavenumbers below $1600\,cm^{-1}$ and at $d(O\cdots O) < 2.50$ Å, strong H bonds are characterized by stretching frequencies between 1600 and $3200\,cm^{-1}$ and $O\cdots O$ distances between 2.50 and 2.70 Å, and weak H bonds occur above $3200\,cm^{-1}$ (up to $\sim 3700\,cm^{-1}$) and at $d(O\cdots O) > 2.70$ Å (with a barely defined upper limit beyond 3 Å) [1].

The correlation of decreasing O–H stretching frequency with enhanced H bonding has early been recognized [2] and attributed to the attractive force of the H bond acceptor which shifts the proton off the donor atom and thus attenuates the O–H bond strength. The relation between frequency shift and H bond lengths has been approached by theoretical calculations, (*e.g.* Ref. [3]) and by comparison of experimentally determined structural and spectroscopic data. One of these early correlations [4] used data with wavenumbers between 1780 and $3700\,cm^{-1}$ and $O\cdots O$ distances between 2.44 and 3.36 Å. At that time the authors assumed a frequency of $3700\,cm^{-1}$ for absence of H bonding, whereas the value for the free OH^- ion accepted today is $\sim 3560\,cm^{-1}$ [5]. A later correlation [6] used a similar data set, typically representing a mixture of organic and inorganic compounds. At this time, however, the extremely broad and low-frequent stretching bands of very strong H bonds had already been accepted and they extended the range of the diagram down to $700\,cm^{-1}$ at $d(O\cdots O) = 2.44$ Å. Whereas the two latter correlations used a wide range of data values at the expense of reduced precision, a recent correlation on solid hydrates [7] provides good precision in a limited frequency range between 2900 and $3600\,cm^{-1}$ and a distance range of $d(O\cdots O) = 2.60$–3.10 Å and $d(H\cdots O) = 1.65$–2.15 Å. In addition, it provides also data for hydrogen bonds with non-oxygen acceptor atoms. The use of selected data (exclusively hydrates, spectra from isotopically diluted samples, only ideal straight H bonds) provides limited scatter and thus it may be used for predictive purposes, assumed that the unknown samples obey to the same quality criteria.

It is the aim of the present paper to present a distance-frequency correlation which provides a wide range of data in terms of $d(O\cdots O)$ or $d(H\cdots O)$ and wavenumber, and which takes data exclusively from inorganic minerals composed of rather abundant elements in nature. It was the intention of the author not to restrict the dataset to a specific group of minerals or to a specific H bond environment. Even if the scatter of data might limit its use for highly accurate predictions, the data should reflect the various deviations from the pure d–v relation which may be encountered in natural solids.

In general, distance-frequency correlations provide important information in cases where bulk crystallographic methods, *e.g.* X-ray and neutron diffraction, are not able to locate protons or O–H$\cdots$O hydrogen bonds. Common examples are trace hydrogen defects [8] and dynamic behavior or disorder of protons in minerals [9, 10]. For the former case only spectroscopic methods allow to determine the distorted environment (*e.g.* distances) around the structural OH defect, for the latter

only the high time resolution of spectroscopic techniques reveals information on the actual proton positions and distances.

Data Selection

In most cases, structural data of minerals were retrieved from the ''Inorganic Crystal Structure Database – ICSD 98/1'' [11] and taken from the references therein. Only for a few minerals a single reference was available. For the majority of compounds a selection among many structure refinements had to be made resulting in a compromise between the most recent reference, the best refined data (using R values), or the experiment with the best H atom localization (usually from neutron diffraction). In many cases only the latter provided data with sufficient accuracy for a $d(\mathrm{H}\cdots\mathrm{O})$ calculation, and only the latter gave accurate angles to classify H bonds into straight or bent ones (with $< \mathrm{O–H}\cdots\mathrm{O} = 150^\circ$ as the critical case). As a rule, H···O distances were rejected if the respective O–H distances were (apparently) shorter than 0.90 Å. In general, room temperature data were used, except for cases with dynamic proton disorder, *e.g.* lawsonite [9] and hemimorphite [12], where the room temperature structure refinements yielded only average disordered positions, whereas the low temperature refinements of the ordered structures gave correct atom sites.

IR spectroscopic data were predominantly retrieved from spectra collections of minerals, *e.g.* Refs [13–15], the most recent one being available also in electronic data format [16]. Transmission spectra of mostly KBr powder pellets were used. In a few cases also single crystal data from oriented sections measured with polarized IR radiation were available. The latter facilitate accurate band assignments even in cases of multiple H bonds using the ratios of polarized band intensities in reconciliation with O–H vector orientations in the structure [17]. In general, in systems with more than one H bond, bands were assigned from low to high wavenumbers to short to long H bond distances, even in cases where a different assignment according to cationic effects had been proposed, *e.g.* malachite [18]. Complicated systems, *e.g.* chalcanthite-$CuSO_4 \cdot 5H_2O$, which display a broad absorption band that cannot be separated into single bands due to a large number of very similar H bonds and vibrational coupling in undeuterated samples, were not included in the correlation.

According to the above mentioned criteria, a number of 65 minerals was finally chosen for the correlation. Mineral names, formulae, structural characteristics, and both structural and spectroscopic references are summed up in Table 1. As far as possible, widely known species were used. Only in a few cases (to cover a rather underrepresented part of the diagram or to set data points of very well studied samples) rare species were included. In cases where minerals display wide and complicated solid solution series, *e.g.* tourmaline, samples close to a well defined endmember composition were used. However, for vesuvianite the crystal chemical environment around the H atoms appeared too variable and complicated to be useful for a reliable correlation.

The samples belong to 5 large groups of compounds: silicates (39 samples, 64 data points), (oxy)hydroxides (8, 12), carbonates (3, 6), sulfates (8, 26), phosphates, and arsenates (7, 17). They contain hydrous species in the form of

Table 1. Mineral names, formulae, structural characteristics, and references for structural and spectroscopic data

Mineral	Formula	Structural elements	Structure	IR data
Mozartite	$CaMnOSiO_3(OH)$	$[SiO_3(OH)]$	[19]	[19]
Topaz	$Al_2(F,OH)_2SiO_4$	$[SiO_4]$	[20]	[21]
Hydrogrossular	$Ca_3Al_2(O_4H_4)_x(SiO_4)_{3-x}$	$[SiO_4]$, $[O_4H_4]$	[22]	[23]
Henritermierite	$Ca_3Mn_2(O_4H_4)(SiO_4)_2$	$[SiO_4]$, $[O_4H_4]$	[24]	[24]
Datolite	$CaBSiO_4(OH)$	$[SiO_4]$	[25]	[16]
Euclase	$BeAl(OH)SiO_4$	$[SiO_4]$	[26]	[14]
Chloritoide	$FeAl_2(OH)_2OSiO_4$	$[SiO_4]$	[27]	[28]
Staurolite	$Fe_4Al_{18}Si_8O_{46}(OH)_2$	$[SiO_4]$	[29]	[30]
Lawsonite	$CaAl_2Si_2O_7(OH)_2 \cdot H_2O$	$[Si_2O_7]$	[9]	[10]
Hennomartinite	$SrMn_2Si_2O_7(OH)_2 \cdot H_2O$	$[Si_2O_7]$	[31]	[10]
Hemimorphite	$Zn_4Si_2O_7(OH)_2 \cdot H_2O$	$[Si_2O_7]$	[12]	[32]
Dehyd. Hemim.	$Zn_4Si_2O_7(OH)_2$	$[Si_2O_7]$	[33]	[33]
Ilvaite	$CaFe_2Fe(OH)OSi_2O_7$	$[Si_2O_7]$	[34]	[35]
Axinite	$Ca_2FeAl_2BO(OH)(Si_2O_7)_2$	$[Si_2O_7]$	[36]	[37]
Bertrandite	$Be_4(OH)_2Si_2O_7$	$[Si_2O_7]$	[38]	[14]
Epidote	$Ca_2(Al,Fe)_3O(OH)Si_2O_7SiO_4$	$[Si_2O_7]$, $[SiO_4]$	[39]	[16]
Clinozoisite	$Ca_2Al_3O(OH)Si_2O_7SiO_4$	$[Si_2O_7]$, $[SiO_4]$	[40]	[16]
Zoisite	$Ca_2Al_3O(OH)Si_2O_7SiO_4$	$[Si_2O_7]$, $[SiO_4]$	[40]	[16]
Pectolite	$Ca_2NaSi_3O_8(OH)$	$[Si_3O_8(OH)]$ chain	[41]	[42]
Serandite	$Mn_2NaSi_3O_8(OH)$	$[Si_3O_8(OH)]$ chain	[43]	[42]
Bazzite	$Be_3Sc_2Si_6O_{18} \cdot xH_2O$,Na	$[Si_6O_{18}]$ ring	[44]	[44]
Beryl	$Be_3Al_2Si_6O_{18} \cdot xH_2O$,Na	$[Si_6O_{18}]$ ring	[45]	[46]
Cordierite	$Mg_2Al_4Si_5O_{18} \cdot xH_2O$,Na	$[Al_2Si_4O_{18}]$ ring	[47]	[48]
Armenite	$BaCa_2Al_6Si_9O_{30} \cdot 2H_2O$	$[Al_3Si_9O_{30}]$ ring	[49]	[49]
Milarite	$KCa_2AlBe_2Si_{12}O_{30} \cdot xH_2O$	$[Si_{12}O_{30}]$ ring	[49]	[49]
Tourmaline	$NaMg_3Al_6(BO_3)_3(OH)_4Si_6O_{18}$	$[Si_6O_{18}]$ ring	[50]	[51]
Tremolite	$Ca_2Mg_5(OH)_2Si_8O_{22}$	$[Si_8O_{22}]$ ribbon	[52]	[53]
Fe-Aktinolite	$Ca_2(Fe,Mg)_5(OH)_2Si_8O_{22}$	$[Si_8O_{22}]$ ribbon	[54]	[55]
Talc	$Mg_3(OH)_2Si_4O_{10}$	$[Si_4O_{10}]$ layer	[56]	[16]
Pyrophyllite	$Al_2(OH)_2Si_4O_{10}$	$[Si_4O_{10}]$ layer	[57]	[16]
Lizardite	$Mg_3(OH)_4Si_2O_5$	$[Si_2O_5]$ layer	[58]	[16]
Kaolinite	$Al_2(OH)_4Si_2O_5$	$[Si_2O_5]$ layer	[59]	[16]
Muscovite	$KAl_2(OH)_2Si_3AlO_{10}$	$[Si_3AlO_{10}]$ layer	[60]	[16]
Phlogopite	$KMg_3(OH)_2Si_3AlO_{10}$	$[Si_3AlO_{10}]$ layer	[61]	[16]
Annite	$KFe_3(OH)_2Si_3AlO_{10}$	$[Si_3AlO_{10}]$ layer	[62]	[63]
Analcime	$NaAlSi_2O_6 \cdot H_2O$	$[(Al,Si)_nO_{2n}]$	[64]	[65]
Natrolite	$Na_2Al_2Si_3O_{10} \cdot 2H_2O$	$[(Al,Si)_nO_{2n}]$	[66]	[16]
Phase A	$Mg_7Si_2O_8(OH)_6$	$[SiO_4]$	[67]	[67]
Phase B	$Mg_{12}Si_4O_{19}(OH)_2$	$[SiO_6]$, $[SiO_4]$	[67]	[67]
Goethite	α-FeOOH	$[FeO_3(OH)_3]$	[68]	[69]
Lepidocrocite	γ-FeOOH	$[FeO_4(OH)_2]$	[14]	[14]
Diaspore	α-AlOOH	$[AlO_3(OH)_3]$	[70]	[71]
Boehmite	γ-AlOOH	$[AlO_4(OH)_2]$	[72]	[14]
Groutite	α-MnOOH	$[MnO_3(OH)_3]$	[71]	[71]
Manganite	γ-MnOOH	$[MnO_3(OH)_3]$	[71]	[71]
Brucite	$Mg(OH)_2$	$[Mg(OH)_6]$	[73]	[14]

Table 1. (*continued*)

Mineral	Formula	Structural elements	Structure	IR data
Gibbsite	$Al(OH)_3$	$[Al(OH)_6]$	[74]	[14]
Trona	$Na_3(CO_3HCO_3) \cdot 2H_2O$	$[CO_3]$, $[CO_2(OH)]$	[75]	[15]
Azurite	$Cu_3(OH)_2(CO_3)_2$	$[CO_3]$	[76]	[18]
Malachite	$Cu_2(OH)_2CO_3$	$[CO_3]$	[77]	[18]
Natrochalcite	$(Na,K)Cu_2(S,Se)O_4 \cdot H_3O_2$	$[(S,Se)O_4]$	[78]	[79]
Antlerite	$Cu_3(OH)_4SO_4$	$[SO_4]$	[80]	[13]
Brochantite	$Cu_4(OH)_6SO_4$	$[SO_4]$	[81]	[18]
Jarosite	$KFe_3(OH)_6(SO_4)_2$	$[SO_4]$	[82]	[13]
Alunite	$KAl_3(OH)_6(SO_4)_2$	$[SO_4]$	[82]	[16]
Natroalunite	$NaAl_3(OH)_6(SO_4)_2$	$[SO_4]$	[83]	[16]
Polyhalite	$K_2Ca_2Mg(SO_4)_4 \cdot 2H_2O$	$[SO_4]$	[84]	[13]
Gypsum	$CaSO_4 \cdot 2H_2O$	$[SO_4]$	[85]	[16]
OH-Apatite	$Ca_5(OH)(PO_4)_3$	$[PO_4]$	[86]	[87]
Lazulite	$(Mg,Fe)Al_2(OH)_2(PO_4)_2$	$[PO_4]$	[88]	[13]
Turquoise	$CuAl_6(OH)_8(PO_4)_4 \cdot 4H_2O$	$[PO_4]$	[89]	[13]
Pseudomalachit	$Cu_5(OH)_4(PO_4)_2$	$[PO_4]$	[90]	[13]
Variscite	$AlPO_4 \cdot 2H_2O$	$[PO_4]$	[91]	[92]
Scorodite	$FeAsO_4 \cdot 2H_2O$	$[AsO_4]$	[93]	[13]
Olivenite	$Cu_2(OH)AsO_4$	$[AsO_4]$	[94]	[13]

Table 2. Compilation of distance and frequency ranges for the three hydrous species H_2O, $H_3O_2^-$, and OH^-

Hydrous species	O···O Distances/Å	Stretching frequencies/cm^{-1}
H_2O	2.59–3.48	2838–3663
$H_3O_2^-$	2.44–2.48[a]	∼1200[a]
OH^-	2.46–3.69	1000–3738

[a] Values for the internal pseudosymmetric H bond of the molecule

OH^-, H_2O, or even $H_3O_2^-$ groups. Table 2 compiles the distance and frequency ranges of these three groups. Thus, H_2O molecules show rather long H bonds and high frequencies, whereas $H_3O_2^-$ units display very low frequencies due to very short H bonds. In contrast, hydroxyl groups are distributed from very strong to very weak H bonds and from very low to very high stretching frequencies.

Results and Discussion

The correlation of d(O···O) *vs*. frequency is plotted in Fig. 1. A data sheet with all relevant distance and wavenumber data can be obtained from the author upon request. The 125 data pairs cover a wavenumber range of 1000 to 3738 cm^{-1} and an O···O distance range of 2.44 to 3.5 Å. Thus, they cover H bonds from very short, almost symmetric ones to very weak H bonds or almost unbonded entities. The plot shows an empty data region between 1500 and 2650 cm^{-1}. This apparently wide gap, however, corresponds to only 2.50 to 2.58 Å in terms of

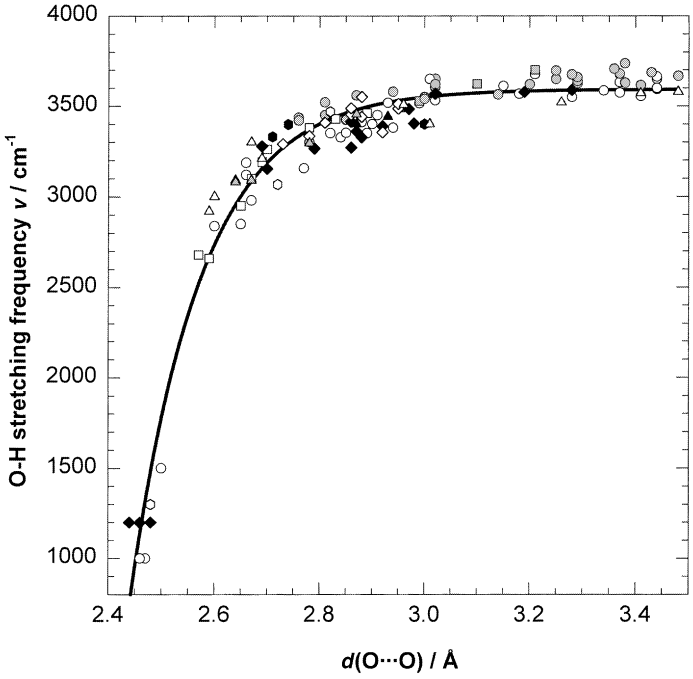

Fig. 1. Plot of the $d(O\cdots O)$ – frequency correlation; open symbols represent straight H bonds, shaded symbols mark bent H bonds, and filled ones denote copper compounds; circles – silicates, squares - (oxy)hydroxides, hexagons – carbonates, diamonds – sulfates, triangles – phosphates and arsenates; the regression curve was calculated for distances < 3.5 Å ($n = 124$) in the form $v = 3592 - 304 \cdot 10^9 \cdot \exp(-d/0.1321)$, $R^2 = 0.96$

distance. A remote datapoint (a copper arsenate) at $d(O\cdots O) = 3.69$ Å (which is evidently far from H bonding and not visible in Fig. 1) was included because of its unusually low stretching frequency of only 3400 cm^{-1}. This feature, as well as the generally wide scatter of data points from copper compounds (solid symbols in Fig. 1) will be discussed below.

The correlation of $d(H\cdots O)$ *vs*. stretching frequency is given in Fig. 2. Because of the above mentioned limitations and lack of sufficiently accurate data, only 47 data pairs are included in the correlation. The low frequency part, representing very strong H bonds, is rather underrepresented and shows extreme scatter. As a matter of fact, the empty wavenumber region is also observed in Fig. 2, and corresponds to a distance range of ~1.45 to 1.60 Å (if the dashed extension line of the regression function is considered representative).

The data of both plots were fitted by a regression function in the form: $v = A - B \cdot \exp \cdot (-d/C)$. A similar function had been employed successfully in a previous correlation [7]. The units of v, A, and B are cm^{-1}, whereas d and C are expressed in Å. A list of resulting regression parameters for all data pairs and for various subgroups is presented in Table 3. For the $d(O\cdots O)$-v correlation the resulting regression coefficients R^2 are better than 0.96 except for the subgroup without the seven very strong H bond data (> 2.55 Å, > 2000 cm^{-1}) where R^2 amounts to only 0.84. It is increased towards 0.98 if the data are restricted in terms of geometry (only straight bonds) or in terms of chemistry (only silicates; no copper

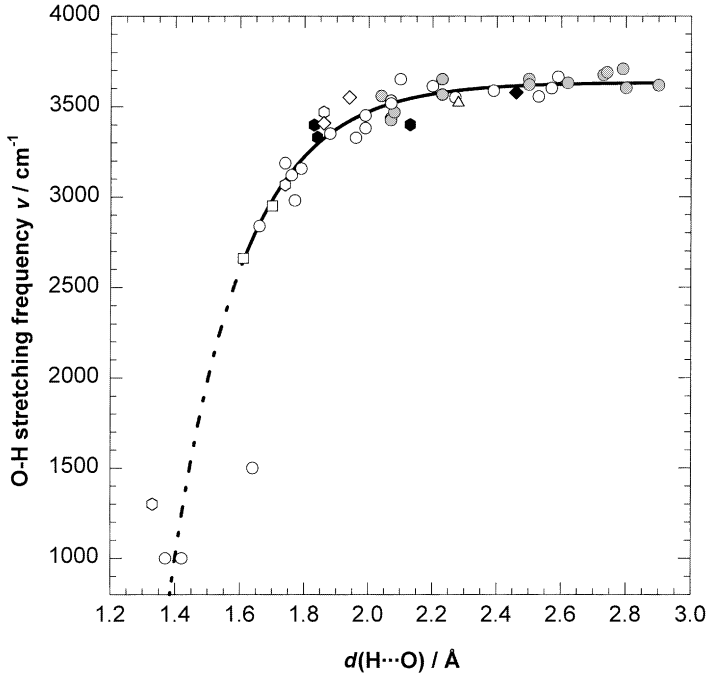

Fig. 2. Plot of the $d(H\cdots O)$ – frequency correlation; symbol code as in Fig. 1; the regression curve was calculated for data above 2500 cm^{-1} ($n = 43$) in the form $v = 3632–1.79 \cdot 10^6 \cdot \exp(-d/0.2146)$, $R^2 = 0.91$, and was extrapolated towards lower frequencies (dashed curve)

Table 3. Parameters of the regression function $v = A - B \cdot \exp(-d/C)$ for all data and for different subgroups; a: $d(O\cdots O)$-v correlation; b: $d(H\cdots O)$-v correlation

a:

Dataset and constraints	n	A/cm^{-1}	B/cm^{-1}	C/Å	R^2
All data	125	3589	$331 \cdot 10^9$	0.1315	0.96
$d < 3.5$ Å[a]	124	3592	$304 \cdot 10^9$	0.1321	0.96
$d \leq 3.2$ Å	95	3545	$1.19 \cdot 10^{12}$	0.1230	0.96
2.55 Å $< d \leq 3.2$ Å	88	3589	$2.97 \cdot 10^9$	0.1706	0.84
Only straight H bonds	80	3554	$635 \cdot 10^9$	0.1270	0.97
Only silicates	64	3622	$238 \cdot 10^9$	0.1346	0.98
Without Cu; $d \leq 3.2$ Å	75	3530	$17.9 \cdot 10^{12}$	0.1088	0.97

b:

Dataset and constraints	n	A/cm^{-1}	B/cm^{-1}	C/Å	R^2
All data	47	3720	$257 \cdot 10^3$	0.2978	0.88
Without $v = 1500$ cm^{-1}	46	3680	$411 \cdot 10^3$	0.2683	0.95
$v > 2500$ cm^{-1}[a]	43	3632	$1.79 \cdot 10^6$	0.2146	0.91
$v > 2500$ cm^{-1}; $d < 2.3$ Å	30	3599	$4.00 \cdot 10^6$	0.1935	0.89
$v > 2500$ cm^{-1}; without Cu	39	3642	$1.38 \cdot 10^6$	0.2227	0.93

[a] Regression curve plotted in Figs. 1 and 2

compounds). For the $d(H\cdots O)$-v correlation R^2 approaches 0.95 if the data point at $v = 1500\,cm^{-1}$ (probably an outlier) is omitted, whereas it is only 0.88 for all 47 data pairs included.

Reasons for scatter of data

A short inspection of Figs. 1 and 2 reveals that deviations from the regression lines may amount to $150\,cm^{-1}$ or even more in some cases. Extreme outliers (*e.g.* among the low-energy data of very strong H bonds in Fig. 2) are distinguished from systematic deviations (*i.e.* data of bent H bonds in Fig. 1), and random scattering that may be strong in certain compounds (*e.g.* Cu minerals) and which is attributed to effects different from H bonding (*e.g.* cationic effects, factor group splitting, dynamic proton behavior).

The most evident outliers occur in Fig. 2 where four data points between 1000 and $1500\,cm^{-1}$ correlate to varying $H\cdots O$ distances between 1.33 and 1.64 Å, even if the expected distance interval (according to the steep slope of the regression line) should be rather narrow. Figure 1 confirms the low wavenumbers, hence the proton-acceptor bond lengths in Fig. 2 must be rather inaccurate. In spite of the quality criteria used (*i.e.* only $O–H > 0.90$ Å), a closer inspection of data reveals that the O–H values from the structure refinements are distorted in some cases. For example, the most severe outlier at $1500\,cm^{-1}$, mozartite [19], passed the quality check with an O–H distance of 0.91 Å (from X-ray data), and thus yielded $d(H\cdots O) = 1.61$ Å. According to a previous d(O–H)-v diagram [6], at a wavenumber of $1500\,cm^{-1}$ an O–H distance of ~1.15 Å is expected. Thus, it is likely that the true data point should be shifted by approximately 0.2 Å to the left. In general, data on very strong H bonds may commonly contain deviations, either in terms of frequency (because of the extremely broad stretching bands) or in terms of proton positions (because of difficulties to refine pseudosymmetric proton sites even with neutrons) [79].

Bent H bonds which yield constantly too high wavenumbers in the $d(O\cdots O)$-v plot (shaded symbols in Fig. 1) are the most important source of systematic deviations. However, this observation is quite reasonable and in good agreement with considerations on bond geometry. The attractive influence of the H bond acceptor is attenuated if the $H\cdots O$ distance in a bent H bond is longer (as a consequence of the bent geometry) than in a straight H bond. As a logical consequence, the $d(H\cdots O)$-v plot in Fig. 2 does not show this systematic scatter towards higher wavenumbers. A sample case is dehydrated hemimorphite [33], where the stretching frequencies of the straight ($3531\,cm^{-1}$) and bent H bonds ($3603\,cm^{-1}$) belong to the same $O\cdots O$ distance of 3.02 Å. The data point for the former is almost exactly on the regression line, whereas the latter is found above the curve in Fig. 1. In contrast, the respective $H\cdots O$ distances, *i.e.* 2.07 Å for the former and 2.80 Å for the latter, are strongly different and thus plot correctly on the regression line in Fig. 2. A different situation is observed in case of bifurcated bonds, where in spite of bent bonds the data point is found at or below the regression line due to the doubled attractive force of the two proton acceptors, *e.g.* datolite, represented by the almost hidden datapoint at 2.96 Å /$3493\,cm^{-1}$ in Fig. 1.

Even though H bonding is extremely weak or absent beyond 3.2 Å (Fig. 1) or 2.3 Å (Fig. 2), data show still appreciable scatter. Hence, these deviations must be caused by effects which are not related to H bonding. Different cationic influences are among the most prominent ones. Starting from the free OH^- ion, stretching frequencies increase by more than $100\,cm^{-1}$ with decreasing metal-oxygen distances in the coordination sphere of the ion [95]. In addition, the hydrogen bond donor strength increases. This synergetic effect is especially strong for copper ions in the coordination sphere of the hydroxyl group [5]. The effect is reversed, if the H bond acceptor is closely coordinated by these metal ions, *e.g.* in malachite, azurite, and brochantite [18]. In general, these effects seem to be the reason for the strong scatter among the copper compounds (solid symbols in Figs. 1 and 2) and even among data of a single mineral (brochantite). The unusually low frequency of $3440\,cm^{-1}$ (without any H bonding) in olivenite appears to be caused also by the peculiar role of copper in the close neighbourhood of the hydroxyl group. Metal ions with different electronegativities in the coordination sphere of the OH^- ion also influence the band positions. This was demonstrated in talc samples ($\nu = 3678\,cm^{-1}$) where Mg was replaced successively by transition metal ions which resulted in a maximum frequency decrease by $50\,cm^{-1}$ for the fully exchanged endmembers [95]. Similar shifts were observed in the amphibole group changing from pure tremolite (Mg) to richterites (K, Fe) [53] and actinolites (Fe) [55].

Factor group splitting (*i.e.* coupling of vibrations in the primitive unit cell) of bands may be another reason for scattered data points. For example, boehmite shows two bands at 3087 and $3283\,cm^{-1}$, whereas the isotopically diluted sample shows only a single band at $3180\,cm^{-1}$ [14]. However, as this rather extreme case demonstrates, vibrational coupling leads to data scattering but not to systematic shifts, as the mean of both coupled modes is quite similar to the uncoupled vibration.

Finally, scatter observed in Fig. 2 may be widely caused by proton dynamics. If O–H vectors show librational or hopping motions, the respective O–H bonds may appear considerably shortened by diffraction methods [22]. For the same reason a d(O–H)-ν correlation was not presented in this paper.

Differences in regression functions

The parameter A of the regression function represents the upper limiting O–H stretching frequency if the H bond acceptor is missing or extremely remote from the proton. Inspection of Table 3a yields A values from 3530 to $3622\,cm^{-1}$ depending upon the dataset constraints. It must be emphasized that predominantly datapoints from bent H bonds which are (almost) not engaged in H bonds (> 3.2 Å), *e.g.* layer and ribbon silicates, display rather high wavenumbers in the upper right corner of Fig. 1. If these distorted values are removed (constraints: "$d \leq 3.2$ Å"; "only straight H bonds"; "without Cu and $d \leq 3.2$ Å"), a limiting wavenumber A between 3530 and $3554\,cm^{-1}$ is approached, which is in excellent agreement with theoretical and experimental values for free OH^- ions, *i.e.* 3554–$3562\,cm^{-1}$ [5]. The highest A value is shown by the "only silicates" subgroup, which is easily explained by the impact of the above mentioned layer and ribbon silicates. The

Table 4. Comparison of calculated data points from regression lines of the present and previous correlation diagrams; distances in Å, wavenumbers in cm^{-1}

$d(O\cdots O)$	*Nakamoto* [4]	*Novak* [6]	*Mikenda* [7]	This study[a]	This study[b]
2.5	2070	1500	–	1758	–
2.6	2500	2680	2880[c]	2732	2870
2.7	2930	3200	3180	3188	3181
2.8	3320	3400	3345	3402	3352
2.9	3490	3500	3450	3503	3447
3.0	3600	–	3510	3550	3499
3.1	3630	–	3550[c]	3572	3528
3.2	3660	–	–	3582	–

[a] All data < 3.5 Å ($n = 124$); [b] only straight H bonds, 2.55 Å < $d \leq$ 3.2 Å ($n = 59$); [c] values slightly outside the data range

curvature of the regression function is expressed by parameter B in the way that high values indicate strong curvature (*i.e.* the subgroup "without Cu") and low values indicate only slight bending (*i.e.* the subgroup "2.55 Å < $d \leq$ 3.2 Å which resembles that of *Mikenda*'s plot [7]).

Figure 2 also contains the high frequency data points in the upper right corner and thus leads to rather elevated A parameters in Table 3b. In addition, due to the strong scatter of the four low frequency data points, regression functions are least-squares fitted only for the part > 2500 cm^{-1} in three cases. Hence, even if H bonds are limited to distances < 2.3 Å, a rather high A value of 3599 cm^{-1} is observed, which resembles that of Table 3a for the region "2.55 Å < $d \leq$ 3.2 Å. The B values, which are lower than in Table 3a, indicate reduced curvature.

Comparison to previous correlation diagrams

To evaluate the present distance-frequency correlation in minerals, the resulting regression lines are compared to published correlation trends. Because of a missing regression function in previous correlations [4, 6] or incompatibility (O–D vibrations in [7]), calculated data pairs across the whole range of H bonds are compiled in Table 4.

Compared to the diagram of *Nakamoto* [4], the present data exceed the old diagram in the low frequency region even if the $d(O\cdots O)$ range is equivalent. Hence, the frequency at 2.5 Å is too high by ~300 cm^{-1}, whereas even the value of 1758 cm^{-1} of the present study appears high compared to the data points used in this region. The high frequency end of *Nakamoto*'s correlation line is also too high by ~100 cm^{-1}, because he assumed a value close to 3700 cm^{-1} for a free OH^- ion. However, his curve is less bent than the present one and so it crosscuts the present line around 2300 and 3500 cm^{-1}. Between these intersections, *Nakamoto*'s data appear too low by more than 200 cm^{-1} (at 2.6 Å). In general, it is a handicap of this previous correlation that it was established from only 26 data points.

Comparison of the present data to the more recent diagram of *Novak* [6] gives excellent agreement between the regression curves. Only the low frequent end of the curve appears too high in the present study (as mentioned above) and might be

better represented by *Novak*'s 1500 cm^{-1} at 2.5 Å. However, his diagram suffers from data restriction to distances below 2.9 Å. The scatter of data appears similar in both correlations, even if *Novak* used only half the number of data of the present correlation curve.

Comparison to the most recent distance-frequency correlation of *Mikenda* [7], who used only high quality data of isotopically diluted solid hydrates, also yields excellent agreement (deviation $\leq 50\,cm^{-1}$). Only *Mikenda*'s data point at 2.6 Å is too high by $\sim 150\,cm^{-1}$. This is a consequence of the curvature of his trend which is rather flat compared to the present regression line. However, the O···O distance of 2.6 Å actually exceeds the data used by this author. To compare further, it appeared challenging to select a high quality data set from the present mineral data that resembles *Mikenda*'s data quite closely. Hence, the distance range was restricted to values between 2.55 and 3.2 Å, and only straight H bonds were used. Table 4 shows that the agreement between the regression lines of these selected data sets is perfect. Deviations amount to only $\sim 10\,cm^{-1}$ except for the point at 3.1 Å (actually outside *Mikenda*'s data [7]), where *Mikenda*'s curve is higher by $\sim 20\,cm^{-1}$. This may be caused by the considerably higher *A* value ($\sim 3650\,cm^{-1}$, converted from O–D to O–H wavenumbers) that was constrained to the frequency of a free HOD molecule in Ref [7].

In general, the more recent distance-frequency correlations [6, 7] are confirmed, and also the trend of a rather old study [4] is met. However, even if full agreement between a restricted dataset of the present study and the high quality data of Mikenda [7] may be obtained, the author is convinced that the complete range of data covering all H bond lengths and frequencies should be used for a true correlation. In contrast to *Mikenda*, the present regression lines as well as that of *Novak* [6] show a stronger curvature to meet the data of very strong H bonds. Moreover, according to visual inspection, a regression line with stronger curvature were easily fitted through *Mikenda*'s data (after release of the constrained *A* parameter) and thus confirms the present distance-frequency correlation in minerals.

Acknowledgements

The critical comments of *A. Beran* (Vienna), *H. Falk* (Linz), and *W. Mikenda* (Vienna) helped to improve the quality of the present paper.

References

[1] Emsley J (1980) Chem Soc Rev **9**: 91
[2] Rundle RE, Parasol M (1952) J Chem Phys **20**: 1487
[3] Bellamy LJ, Owen AJ (1969) Spectrochim Acta **A25**: 329
[4] Nakamoto K, Margoshes M, Rundle RE (1955) J Am Chem Soc **77**: 6480
[5] Lutz HD (1995) Struct Bond **82**: 85
[6] Novak A (1974) Struct Bond **18**: 177
[7] Mikenda W (1986) J Mol Struct **147**: 1
[8] Bell DR, Rossman GR (1992) Contrib Mineral Petrol **111**: 161
[9] Libowitzky E, Armbruster T (1995) Am Mineral **80**: 1277
[10] Libowitzky E, Rossman GR (1996) Am Mineral **81**: 1080

[11] ICSD 98/1 Inorganic Crystal Structure Database, FIZ Karlsruhe – Gmelin Institute
[12] Libowitzky E, Schultz AJ, Young DM (1998) Z Kristallogr **213**: 659
[13] Moenke H (1966) Mineralspektren II. Akademie-Verlag, Berlin
[14] Farmer VC (ed) (1974) The Infrared Spectra of Minerals. Miner Soc, London
[15] Jones GC, Jackson B (1993) Infrared Transmission Spectra of Carbonate Minerals. Chapman & Hall, London
[16] Salisbury JW, Walter LS, Vergo N, D'Aria DM (1992) Infrared (2.1–25 μm) Spectra of Minerals. Johns Hopkins, London
[17] Libowitzky E, Rossman GR (1996) Phys Chem Minerals **23**: 319
[18] Schmidt M, Lutz HD (1993) Phys Chem Minerals **20**: 27
[19] Nyfeler D, Hoffmann C, Armbruster T, Kunz M, Libowitzky E (1997) Am Mineral **82**: 841
[20] Zobetz E, Zemann J, Heger G, Voellenkle H (1979) Anz Österr Akad Wiss, Math-Naturwiss Kl **116**: 145
[21] Shinoda K, Aikawa N (1994) Phys Chem Minerals **21**: 24
[22] Lager GA, Armbruster T, Faber J (1987) Am Mineral **72:** 756
[23] Rossman GR, Aines RD (1991) Am Mineral **76**: 1153
[24] Armbruster T, Libowitzky E, Kunz M, Miletich R, Gutzmer J (1999) Am Mineral **84** (in preparation)
[25] Foit FF Jr, Phillips MW, Gibbs GV (1973) Am Mineral **58**: 909
[26] Hazen RM, Au AY, Finger LW (1986) Am Mineral **71**: 977
[27] Hanscom RH (1975) Acta Cryst **B31**: 780
[28] Fransolet A-M (1978) Bull Minéral **101**: 548
[29] Ståhl K, Kvick Å, Smith JV (1988) J Sol State Chem **73**: 362
[30] Koch-Müller M, Langer K, Beran A (1995) Phys Chem Minerals **22**: 108
[31] Libowitzky E, Armbruster T (1996) Am Mineral **81**: 9
[32] Libowitzky E, Rossman GR (1997) Eur J Mineral **9**: 793
[33] Libowitzky E, Kohler T, Armbruster T, Rossman GR (1997) Eur J Mineral **9**: 803
[34] Ghose S, Hewat AW, Marezio M (1984) Phys Chem Minerals **11**: 67
[35] Beran A, Bittner H (1974) Tscherm Min Petr Mitt **21**: 11
[36] Swinnea JS, Steinfink H, Rendon Diaz Miron LE, de la Vega SE (1981) Am Mineral **66**: 428
[37] Beran A (1971) Tscherm Min Petr Mitt **16**: 281
[38] Downs JW, Ross FK (1987) Am Mineral **72**: 979
[39] Nozik YZ, Kanepit VN, Fykin LY, Makarov YS (1978) Geochem Internat **15**: 66
[40] Comodi P, Zanazzi PF (1997) Am Mineral **82**: 61
[41] Takéuchi Y, Kudoh Y (1977) Z Kristallogr **146**: 281
[42] Hammer VMF, Libowitzky E, Rossman GR (1998) Am Mineral **83**: 569
[43] Jacobsen SD (1998) PhD Thesis, University of Colorado, Boulder
[44] Armbruster T, Libowitzky E, Diamond L, Auernhammer M, Bauerhansl P, Hoffmann C, Irran E, Kurka A, Rosenstingl H (1995) Miner Petrol **52**: 113
[45] Artioli G, Rinaldi R, Ståhl K, Zanazzi PF (1993) Am Mineral **78**: 762
[46] Aurisicchio C, Grubessi O, Zecchini P (1994) Can Mineral **32**: 55
[47] Wallace JH, Wenk HR (1980) Am Mineral **65**: 96
[48] Aines RD, Rossman GR (1984) Am Mineral **69**: 319
[49] Armbruster T (1999) Am Mineral **84**: 92
[50] Hawthorne FC, MacDonald DJ, Burns PC (1993) Am Mineral **78**: 265
[51] Gonzalez-Carreño T, Fernández M, Sanz J (1988) Phys Chem Minerals **15**: 452
[52] Yang H-X, Evans BW (1996) Am Mineral **81**: 1117
[53] Gottschalk M, Andrut M (1998) Phys Chem Minerals **25**: 101
[54] Urusov VS, Zver'kova ON, Yamnova NA, Polosin AV (1987) Vestnik Moskovskogo Universiteta, Geologiya **1987**: 43
[55] Skogby H, Rossman G (1991) Phys Chem Minerals **18**: 64

[56] Perdikatsis B, Burzlaff H (1981) Z Kristallogr **156**: 177
[57] Lee JH, Guggenheim S (1981) Am Mineral **66**: 350
[58] Gregorkiewitz M, Lebech B, Mellini M, Viti C (1996) Am Mineral **81**: 1111
[59] El Sayed K, Heiba ZK, Abdel Rahman AM (1990) Cryst Res Tech **25**: 305
[60] Catti M, Ferraris G, Hull S, Pavese A (1994) Eur J Mineral **6**: 171
[61] Rayner JH (1974) Min Mag **39**: 850
[62] Hazen RM, Burnham CW (1973) Am Mineral **58**: 889
[63] Redhammer GJ, Beran A, Dachs E, Amthauer G (1993) Phys Chem Minerals **20**: 382
[64] Ferraris G, Jones DW, Yerkess J (1972) Z Kristallogr **135**: 240
[65] Libowitzky E, Rossman GR (1997) Am Mineral **82**: 1111
[66] Stuckenschmidt E, Joswig W, Baur WH (1993) Phys Chem Minerals **19**: 562
[67] Hofmeister AM, Cynn H, Burnley PC, Meade C (1999) Am Mineral **84**: 454
[68] Szytula A, Burewicz A, Dimitrijewic Z, Krasnicki S, Rzany H, Todorovic J, Wanic A, Wolski W (1968) Phys Stat Sol **26**: 429
[69] Libowitzky E (1996) Mitt Österr Miner Ges **141**: 134
[70] Hill RJ (1979) Phys Chem Minerals **5**: 179
[71] Kohler T, Armbruster T, Libowitzky E (1997) J Solid State Chem **133**: 486
[72] Christoph GG, Corbato CE, Hofmann A, Tettenhorst RT (1979) Clays Clay Miner **27**: 81
[73] Zigan F, Rothbauer R (1967) N Jb Miner Mh **1967**: 137
[74] Saalfeld H, Wedde M (1974) Z Kristallogr **139**: 129
[75] Pertlik F (1986) Mitt Österr Miner Ges **131**: 7
[76] Zigan F, Schuster HD (1972) Z Kristallogr **135**: 416
[77] Zigan F, Joswig W, Schuster HD (1977) Z Kristallogr **145**: 412
[78] Giester G (1989) Z Kristallogr **187**: 239
[79] Beran A, Giester G, Libowitzky E (1997) Mineral Petrol **61**: 223
[80] Hawthorne FC, Groat LE, Eby RK (1989) Can Mineral **27**: 205
[81] Helliwell M, Smith JV (1997) Acta Cryst **C53**: 1369
[82] Menchetti S, Sabelli C (1976) N Jb Miner Mh **1976**: 406
[83] Okada K, Hirabayashi J, Ossaka J (1982) N Jb Miner Mh **1982**: 534
[84] Schlatti M, Sahl K, Zemann A, Zemann J (1970) Tscherm Min Petr Mitt **14**: 75
[85] Pedersen BF, Semmingsen D (1982) Acta Cryst **B38**: 1074
[86] Hughes JM, Cameron M, Crowley KD (1989) Am Mineral **74**: 870
[87] Engel G, Klee WE (1972) J Solid State Chem **5**: 28
[88] Giuseppetti G, Tadini C (1983) N Jb Miner Mh **1983**: 410
[89] Cid-Dresdner H (1965) Z Kristallogr **121**: 87
[90] Shoemaker GL, Anderson JB, Kostiner E (1981) Am Mineral **66**: 169
[91] Kniep R, Mootz D, Vegas A (1977) Acta Cryst **B33**: 263
[92] Salvador Salvador P, Fayos J (1972) Am Mineral **57**: 36
[93] Hawthorne FC (1976) Acta Cryst **B32**: 2891
[94] Toman K (1977) Acta Cryst **B33**: 2628
[95] Beckenkamp K, Lutz HD (1992) J Mol Struct **270**: 393

Received November 9, 1998. Accepted (revised) December 8, 1998